

Check for updates

Mg Substitution Improves the Surface Stability of High-Voltage Spinel Cathodes under Accelerated Aging Conditions

Beth E. Murdock, Liang Zhao, Ashok S. Menon, Samuel G. Booth, Jack Fitzpatrick, Li Zhang, Louis F. J. Piper, Serena A. Cussen, and Nuria Tapia-Ruiz*

LiNi_{0.5}Mn_{1.5}O₄ (LNMO) cathodes offer a cobalt-free, high-voltage alternative to current state-of-the-art Li-ion battery cathodes, and are particularly well-suited for high-power applications due to their 3D lithium-ion pathways and structural stability. However, degradation of commercial electrolytes at high voltages exacerbates capacity decay, as instability at the cathode surface causes active material loss, surface reconstructions, thickening surface layers, and increases in internal cell resistance. Cationic substitution has been proposed to enhance surface stability, thus limiting capacity decay. Here, we demonstrate the stabilizing effect of Mg on the LNMO cathode surface, which is most evident during the early stages of cycling. This study indicates that improved O 2p-TM 3d hybridization in Mg-substituted LNMO, facilitated by Li-site defects, leads to the formation of a stable surface layer that is corrosion-resistant at high voltage. Examination of Fe-substituted and unsubstituted LNMO further confirms that the surface stability is uniquely enabled by Mg substitution. This work offers valuable insights into surface design for reducing degradation in high-voltage spinel cathodes.

1. Introduction

Future energy storage demands require the development of reliable, high-energy-density Li-ion batteries. As a result, next-generation cathode materials are seeing a push toward higher

voltage operation, allowing for higher energy densities. By extending the upper voltage limit of the cathode, however, we also push the limits of conventional carbonate-based electrolytes, which are known to degrade at V > 4.2 V vs. Li^+/Li . This is a cause for concern for high-voltage spinel cathodes ($\text{LiNi}_{0.5}\text{Mn}_{1.5}\text{O}_4$, LNMO) with redox reactions occurring as high as 4.75 V, which, despite their high theoretical energy density (650 Wh kg^{-1}), experience poor cycling stability. [2]

This poor cycling stability of LNMO cathodes is attributed to electrolyte degradation at high voltages: a complex phenomenon that coincides with the dissolution of active transition metal (TM) ions from the cathode particles. For example, dissolution of Ni²⁺ and Mn²⁺ ions has been observed after both storage and cycling of LNMO cells.^[3] This not only results in the loss of cathode active material, but the dissolution

of Mn^{2+} ions is particularly problematic in destabilizing the anode surface layer, causing capacity decay.^[3] Studies have shown that the high-voltage surface reconstruction of LNMO occurs when reduced transition metals migrate into the delithiated tetrahedral sites, forming a Mn_3O_4 -like surface and thus a source of

B. E. Murdock
Department of Chemistry
Lancaster University
Lancaster LA1 4YB, UK
B. E. Murdock, L. Zhao, J. Fitzpatrick, L. Zhang, N. Tapia-Ruiz
Department of Chemistry
Molecular Sciences Research Hub

Imperial College London White City Campus, London W12 0BZ, UK E-mail: n.tapia-ruiz@imperial.ac.uk

The ORCID identification number(s) for the author(s) of this article can be found under https://doi.org/10.1002/adfm.202501660

© 2025 The Author(s). Advanced Functional Materials published by Wiley-VCH GmbH. This is an open access article under the terms of the Creative Commons Attribution License, which permits use, distribution and reproduction in any medium, provided the original work is properly cited.

DOI: 10.1002/adfm.202501660

B. E. Murdock, L. Zhao, A. S. Menon, S. G. Booth, J. Fitzpatrick, L. Zhang, L. F. J. Piper, S. A. Cussen, N. Tapia-Ruiz The Faraday Institution, Quad One

The Faraday Institution, Quad One Harwell Science and Innovation Campus Didcot OX11 0RA, UK

A. S. Menon, L. F. J. Piper Warwick Manufacturing Group University of Warwick Coventry CV4 7AL, UK

S. G. Booth
Department of Materials Science and Engineering
The University of Sheffield
Sir Robert Hadfield Building, Sheffield S1 3 D, UK

S. A. Cussen School of Chemistry University College Dublin Belfield, Dublin 4, Dublin D04 C1P1, Ireland



www.afm-journal.de

 Mn^{3+} ions.^[4,5] Surface Mn^{3+} ions can then undergo HF-driven disproportionation to form surface λ -MnO₂ and dissolved Mn^{2+} ions. This is consistent with reports indicating the presence of HF in the electrolyte (at $V \approx 4.68~V$ vs. Li^+/Li) before the detection of Mn^{2+} ions.^[4]

Electrolyte degradation at the cathode is strongly influenced by the oxidative stability of the electrolyte solvent. In a conventional Li-ion cell, carbonate-based solvents such as ethylene carbonate (EC) typically oxidize at V > 4.2 V. Such an oxidation reaction produces a series of organic oligomers (e.g., polycarbonates and polyethylene oxide moieties) and organofluorine species, alongside H₂O and other highly acidic species.^[6,7] This causes the hydrolysis of the LiPF₆ salt, forming HF, LiF, POF₃, and various Li_PO_F_ species via subsequent reactions. [6,7] HF formation is followed by HF-etching of the cathode surface, resulting in the loss of active material and the subsequent production of additional H₂O, perpetuating a continuous cycle of degradation, as outlined above.^[7] A build-up of degradation species at the cathode surface forms a surface laver known as the cathode-electrolyte interphase (CEI). In some cases, the presence of a stable CEI on the surface can help prevent continuous electrolyte degradation. [8,9] However, the CEI layer formed on the LNMO surface is typically unstable, resulting in CEI thickening, impeded Li+ diffusion, and progressive active material depletion.^[8,9] HF is also problematic for the stability of aluminum current collectors, as HF corrosion, particularly during high-voltage operation, has been shown to form an insulating layer of AlF₃. Although this layer can initially passivate the current collector, excessive growth increases the contact resistance between the cathode and current collector, increasing cell impedance.[10]

Many studies on LNMO cathodes focus on reducing degradation and dissolution at the electrode surface at high voltages using strategies such as surface coatings, high-voltage electrolytes/additives, particle engineering, and elemental substitution. [2,11,12] Among these, cationic substitution on the Ni site with inexpensive and Earth-abundant elements, such as Fe and Mg, has the potential to improve performance, increase structural stability, and lower overall cathode costs.

Previous studies have demonstrated that replacing Ni with Fe or Mg ions can improve the cycling stability of LNMO, with some reports hypothesizing that the migration of substituent ions to the surface contributes to increased stability by facilitating the formation of a more robust and stable cathode–electrolyte interphase (CEI). [13–15] Mg substitution has been shown to suppress $\rm Mn^{2+}$ dissolution at high voltages, which is a critical degradation mechanism for LNMO cathodes. This suppression has been attributed to the presence of Li-site defects in Mg-substituted LNMO, which help prevent the high-voltage surface reconstruction that typically leads to Mn dissolution. [13]

Our earlier work confirmed the presence of Li-site defects in Mg-substituted LNMO.^[16] In comparison, Fe substitution produces fewer Li-site defects, while unsubstituted LNMO has negligible defect concentrations. Despite differences in defect chemistry, initial cycling tests under ambient conditions showed comparable capacity retention for Mg- and Fe-substituted, and unsubstituted LNMO samples (96% after 300 cycles, 1C, 3.5–4.9 V, half-cell vs. Li⁺/Li).^[16] To assess the effect of substitution on surface stability, accelerated aging conditions are therefore required.

This study evaluates the electrochemical performance of $\text{LiNi}_{0.5-x}\text{M}_x\text{Mn}_{1.5}\text{O}_4$ (M = Fe and Mg; x=0–0.05) at elevated cycling temperatures (50 °C). The CEI of unsubstituted, Mg-substituted, and Fe-substituted LNMO is investigated using a combination of synchrotron hard X-ray photoelectron spectroscopy (HAXPES) and soft X-ray absorption spectroscopy (sXAS) collected in the total electron yield (TEY) mode, while changes in cell impedance are tracked using electrochemical impedance spectroscopy (EIS). Our findings from experiments on Mg- and Fe-substituted LNMO demonstrate the stabilizing effect of Mg on the cathode surface, allowing for improved performance under accelerated aging conditions. Fe, on the other hand, leads to minimal improvements in both capacity retention and surface stability.

2. Electrochemical Performance

As reported in our earlier work, LNMO prepared using a coprecipitation method with oxalic acid shows high rate performance and capacity retention under ambient conditions of $\approx 96\%$ in a half-cell after 300 cycles at 1C (28 °C, 3.5–4.9 V). [16] After an initial increase in capacity, LNMO achieves a peak capacity of \approx 125 mAh g $^{-1}$. At elevated temperatures, which are used to accelerate aging, the capacity retention decreases to $\approx 86\%$ after 300 cycles (50 °C, 1C, 3.5–4.9 V, **Figure 1a**).

To improve the high-temperature capacity retention of LNMO, several substituted spinel samples of composition $\mathrm{LiNi}_{0.5-x}\mathrm{M}_x\mathrm{Mn}_{1.5}\mathrm{O}_4$ (M = Fe and Mg; x=0–0.2) were prepared (Figure S1, Supporting Information). While all substituted samples showed improvements in high-temperature capacity retention, only those with low substituent concentrations provided improvements without a substantial loss of initial capacity (i.e., x=0.05, Figure S1a–c, Supporting Information). As a result, this work focuses on understanding the performance of $\mathrm{LiNi}_{0.5}\mathrm{Mn}_{1.5}\mathrm{O}_4$ (LNMO), $\mathrm{LiNi}_{0.45}\mathrm{Fe}_{0.05}\mathrm{Mn}_{1.5}\mathrm{O}_4$ (Fe0.05), and $\mathrm{LiNi}_{0.45}\mathrm{Mg}_{0.05}\mathrm{Mn}_{1.5}\mathrm{O}_4$ (Mg0.05) at 50 °C.

At 50 °C, the initial discharge capacities of LNMO, Fe0.05, and Mg0.05 are comparable (≈ 130 mAh g⁻¹, Figure 1a). However, Mg0.05 shows improved capacity retention after 300 cycles when compared to Fe0.05 and LNMO (94%, 88%, and 86%, respectively) (Figure 1a). Spinel/graphite full-cells were cycled at 50 °C to further validate the improvement provided by Mg substitution (Figure S2, Supporting Information, 1C, 2.9–4.75 V, 30 cycles). In a full-cell, Mg0.05 has higher capacity retention (88%) than LNMO (84%) and Fe0.05 (82%), which is consistent with the trends in half-cell data, indicating that the stabilization effect persists under more realistic operating conditions. While full-cell data confirm that Mg substitution enhances capacity retention, half-cell testing is still necessary for identifying cathode-specific effects. As a result, we concentrated on half-cell data to further investigate the mechanisms underlying improved performance.

To gain a better understanding of the rate at which the capacity degrades, the capacity retention (CR) from cycle to cycle is shown (Equation 1, Figure 1c), with insets highlighting the differences observed during initial cycling (cycles 1–50) and long cycling (cycles 200–300).

$$CR = \left(\frac{C_{n+1}}{C_n}\right) \times 100 \tag{1}$$

16163028, 0, Downloaded from https://advanced.onlinelibrary.wiley.com

, Wiley Online Library on [10/11/2025]. See the Terms

nditions) on Wiley Online Library for rules of use; OA articles are governed by the applicable Creative Commons

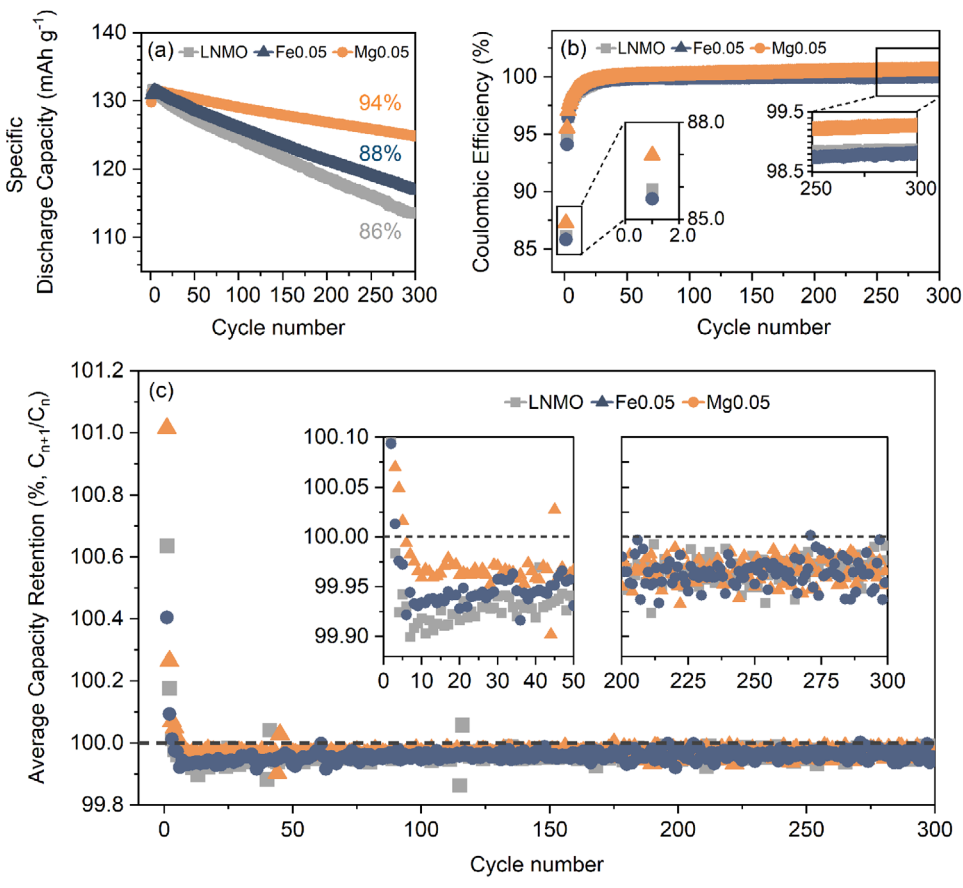


Figure 1. Long-term cycling performance of spinel/Li half-cells at 50 °C (1C, 3.5-4.9 V): a) cycling stability and b) corresponding coulombic efficiency values of LNMO (grey), Mg0.05 (orange), and Fe0.05 (blue) over 300 cycles; and c) average cycle-to-cycle variations in capacity retention ($CR = (\frac{C_n + 1}{C_n}) \times (C_n + C_n)$ 100), calculated from a minimum of 3 cells. Insets highlight the different rates of degradation from cycles 1–50 and 200–300.

All samples have initial CR values > 100%, indicating a slight increase in capacity over the first 5 cycles: a result of half-cell cycling in this system, which allows for gradual activation of lithium storage sites (Note S1, Supporting Information). After activation, capacity starts to degrade (CR < 100%). From cycles 10-50, the CR is highest for Mg0.05 (\approx 99.97%), followed by Fe0.05 (\approx 99.95%) and LNMO (\approx 99.92%). While these differences may appear minor, capacity loss increases exponentially with cycle number, since the total capacity retention is the product of CR from cycle 1 to cycle n (Equation 2).

$$\prod_{i=1}^{n} CR_{i} \tag{2}$$

This suggests that the rate of capacity degradation increases from Mg0.05 < Fe0.05 < LNMO. However, after initial cycling (i.e., > 50 cycles), the cycle-to-cycle variation in capacity is comparable across all three samples. We, therefore, attribute the enhanced long-term performance of Mg0.05 to the improved stability during the first 50 cycles. This suggests that Mg substitution in LNMO can partially alleviate degradation processes, which are most severe during the initial stages of cycling.

To understand the role of unwanted oxidation processes in the observed differences in cycling stability, we compared the coulombic efficiency values (CE) of these materials. Low CE in LNMO-based full-cells is linked to the loss of cyclable Li due to anode interphase instability caused by dissolved Mn²⁺ ions. [17,18] However, unlike full-cells, half-cells have a large Li inventory provided by the lithium counter electrode. As a result, spinel/Li halfcells are limited by cathode sites rather than lithium inventory.^[19] In other words, the capacity is primarily determined by the amount of lithium that can be inserted into the cathode rather than the loss of Li. As outlined by Tornheim et al., coulombic efficiency in site-limited cells is influenced by the oxidation current, I_{ox} , where increases in I_{ox} (through electrolyte oxidation, O₂ loss, or current collector corrosion) can contribute to an increase in charge capacity and a decrease in discharge capacity.^[19] This results in lower CE at any given cycle.

All samples have low initial CE, indicating that the cathode experiences a significant amount of unwanted oxidation during the first cycle. However, initial CE is marginally higher for Mg0.05 (\approx 87%) when compared to LNMO and Fe0.05 (\approx 86%, Figure 1b). Despite low initial CE values, all samples show an increase in CE over the first 20 cycles, leveling off at 99.2% for Mg0.05 and 98.8% for both LNMO and Fe0.05. This demonstrates that unwanted oxidation processes at the cathode surface are most severe during initial cycling, which could explain the faster rate of capacity degradation observed during the first 50 cycles (Figure 1c). Furthermore, by the 300th cycle, the CE for Mg0.05 is only 0.4%



www.afm-journal.de

higher than in LNMO, compared to a 1% improvement on the first cycle, indicating that the presence of Mg in LNMO has the greatest influence during initial cycling. Despite improvements, both half-cell and full-cell CEs for all samples remain lower than those required to meet full-cell industry standards (>99.96%, full-cell, Figure S2, Supporting Information). While the use of elevated temperatures in this work is expected to accelerate processes that contribute to I_{ox} , resulting in lower CE, half-cell CE values at ambient temperatures are still less than ideal (99.1–99.6%, Figure S1d, Supporting Information).

The charge/discharge voltage profiles provide insight into the degradation of LNMO, Fe0.05, and Mg0.05, with two high-voltage charge plateaux at \approx 4.7 and 4.75 V, and a lower voltage charge plateau at \approx 4 V (**Figure 2a–c**). These plateaux correspond to redox reactions related to the Ni²+/3+, Ni³+/4+, and Mn³+/4+ redox couples, respectively. [21] The concentration of Mn³+ ions in these samples increases with Fe and Mg concentration, resulting in unit cell expansion, as confirmed by diffraction data from our previous work. [16]

Increased Mn3+ ion concentrations are expected for Fesubstituted LNMO samples to maintain charge neutrality when Ni²⁺ ions are replaced with Fe³⁺ ions. Conversely, when Ni²⁺ ions are replaced with Mg2+ ions, Mn3+ ions are not expected since the charge distribution remains unchanged. However, our previous work revealed that Mn3+ ions in Mg-substituted LNMO samples charge balance cation deficiencies in the main spinel phase caused by impurity phase formation. Furthermore, we found a strong correlation between the formation of Licontaining impurity phases and the formation of Li-site defects (Mg or Fe on the Li site), the concentration of which was higher in Mg-substituted samples than in analogous Fe-substituted samples. [16] The presence of Li-site defects has been shown to prevent surface reconstruction.[13] Despite the larger concentration of Li-site defects in Mg0.05, Fe0.05 has a higher concentration of Mn3+ ions than Mg0.05, as evidenced by the longer 4 V plateau. High concentrations of Mn³⁺ ions are frequently reported to have adverse effects on cycling stability due to the infamous Mn³⁺ ion disproportionation and subsequent Mn²⁺ ion dissolution, which could explain why Fe0.05 has the lowest capacity retention in a full-cell (Figure S2, Supporting Information).^[22]

Differential capacity plots show well-defined peaks at 4, 4.7, and 4.75 V, which correspond to the plateaux observed in the voltage profiles (Figure 2d-i). Differential capacity in the 4 V region can be used to identify differences in Mn redox behavior. The 4 V discharge peak for LNMO and Fe0.05 increases from cycles 1-50, while the 4 V charge peak decreases (Figure 2g,h). This can be attributed to Mn³⁺ ion disproportionation, which can result in the formation of electrochemically active Mn⁴⁺ ions (e.g., as MnO₂ phases) and soluble Mn²⁺ ions, the latter of which dissolves into the electrolyte and is irreversibly lost. As a result, the redox-active Mn3+ centres are depleted, explaining the diminishing charge peak, while the newly formed MnO₂ continues to contribute to the discharge process, leading to the increased discharge peak. From cycles 50-300, the 4 V peak intensities for LNMO and Fe0.05 remain relatively constant, suggesting that disproportionation is most severe during the first 50 cycles. In contrast, for Mg0.05, both the 4 V charge and discharge peaks show a subtle decrease in intensity. This simultaneous decrease in intensity in both the charge and discharge peaks indicates that electrochemically active Mn^{4+} ions are not formed to the same extent, implying that Mn^{3+} disproportionation is less pronounced. Loss of intensity may be better correlated with a subtle loss of active Li. Suppressed Mn^{3+} ion disproportionation is expected to contribute to the improved cycling stability of Mg0.05, particularly in full-cells (Figure S2, Supporting Information).

The high-voltage peaks at 4.7 and 4.75 V also experience a loss in intensity after 300 cycles, and may be explained by i) loss of active Ni/Li ions through dissolution and parasitic surface reactions or ii) inhibited Li⁺ transport, preventing full oxidation/reduction of Ni.[17,18] In addition to intensity changes, all three samples exhibit voltage polarization, as evidenced by shifts in peak positions relative to those observed in cycle 1. Such voltage polarization indicates an increase in internal cell resistance, which could be caused by a combination of surface layer resistance, chargetransfer resistance, and contact resistance, all of which can lead to poor electrode kinetics.[23] While all samples experience voltage polarization and changes in peak intensity, the LNMO sample exhibits the most significant changes. Polarization in Fe0.05, on the other hand, is reduced, while Mg0.05 shows greater stability in both voltage and capacity. The improved stability of Mg0.05 suggests that Mg substitution can prevent capacity fade while also mitigating voltage decay and increases in cell impedance.

The compiled electrochemical characterization suggests that the Mg0.05 sample may experience less electrolyte degradation, loss of active material, and changes in internal cell resistance during prolonged cycling under accelerated aging conditions. The electrochemical evaluations of Fe0.05, on the other hand, suggest that it degrades similarly to LNMO. To further investigate these differences, ex situ surface analysis and electrochemical impedance spectroscopy were used.

3. Surface Analysis

Ex situ surface analyses were carried out on spinel electrodes extracted from spinel/Li half-cells to determine the effect of Fe and Mg substitution on electrolyte degradation and surface stability of LNMO. The half-cell configuration allows for a more direct assessment of cathode-specific degradation mechanisms by removing effects caused by anode-side reactions. The spinel electrode surfaces were analyzed at various stages of cycling: in the pristine state (P); after soaking in the electrolyte for 12 h (OCV); and at the end of cycles 1, 150, and 300. Electrodes made of carbon black and PVDF (CB/PVDF) soaked in the electrolyte were also analyzed to elucidate the role of inactive components in the chemical degradation of the electrolyte. Samples are labelled using the notation S-C (sample-charge state), where S = CB/PVDF, LNMO, Fe0.05, or Mg0.05, and C = P, OCV, 1, 150, or 300. Each electrode was analyzed using both soft X-ray absorption spectroscopy in total electron yield mode (sXAS-TEY, < 1 keV) and hard X-ray photoelectron spectroscopy (HAXPES, 2.2 keV).

3.1. Hard X-Ray Photoelectron Spectroscopy

In the C 1s, O 1s, and F 1s HAXPES spectra, the CB/PVDF-P electrode shows peaks characteristic of both CB and PVDF (Figure S3, Supporting Information). The C 1s peak at 284.4 eV can be

Wiley Online Library on [10/11/2025]. See the

www.afm-journal.de

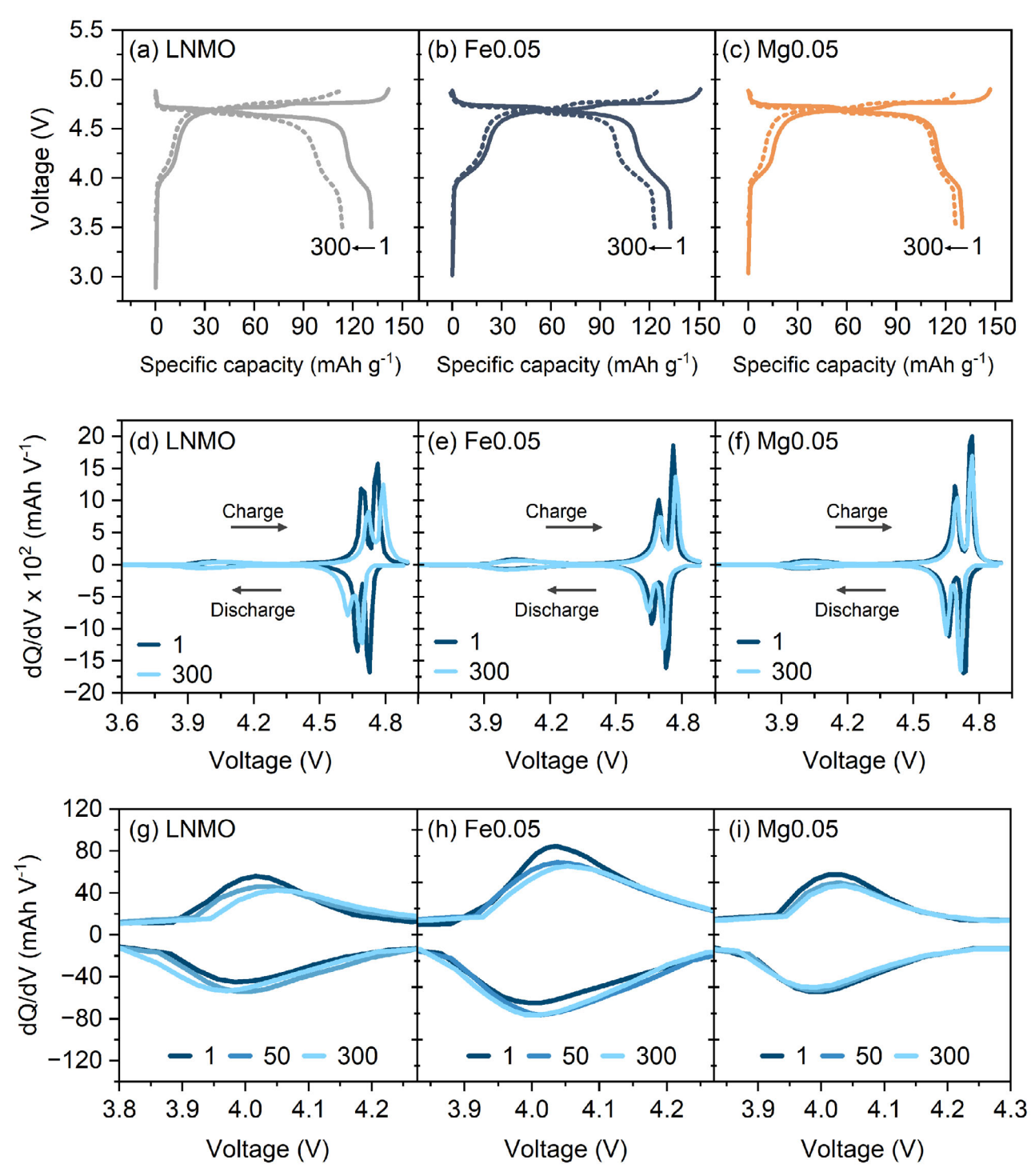


Figure 2. Voltage profiles of the first (solid) and 300th cycle (dashed) for a) LNMO, b) Fe0.05, and c) Mg0.05, obtained at 50 °C (1C, 3.5-4.9 V; dO/dV vs. V plots corresponding to cycles 1 and 300 for d) LNMO, e) Fe0.05, and f) Mg0.05); enlarged dQ/dV vs. V plot in the 4 V region, mapping the evolution of Mn^{3+/4+}-related capacity from cycles 1–300 for g) LNMO, h) Fe0.05, and i) Mg0.05.

attributed to the sp² carbon of CB.^[24] As expected, the CB surface is slightly oxidized, with corresponding peaks in the C 1s and O 1s spectra at 287.5 and 531.5 eV (C=O) and 286 and 532.5 eV (C-O/O-H). Additional C 1s peaks at 286.2 and 290.8 eV are attributed to the CH2 and CF2 groups of the PVDF binder, respectively, and the presence of the peak at 687.8 eV indicates the C—F bonding in the F 1s spectra.^[25]

LNMO-P, Fe0.05-P, and Mg0.05-P show peaks consistent with PVDF and oxidized CB, as well as some noteworthy changes in the spectra. The electrodes with active material show a lower





www.afm-journal.de

intensity C—C (sp²) peak in the C 1s spectra due to the lower concentration of CB in the electrode formulation than that of the CB/PVDF-P electrode (10% vs. 90%). The C 1s spectra are otherwise comparable, suggesting that CB on the surface of each electrode is oxidized to a similar extent. As a result, similarities in the O 1s spectra at 531.5 and 532.5 eV are expected. However, the peak at 532.5 eV is more intense for electrodes containing active material, indicating the presence of a non-carbon functional group. The TM-OH terminating group on the cathode surface is more likely responsible for the increase in peak intensity, as reported elsewhere.^[4] While surface hydroxyl groups can accelerate the production of HF, the hydroxyl concentration is similar across all samples.[26] In addition to TM-OH bonding, TM-O bonding from the spinel lattice is also observed in the O 1s spectra at ≈ 529 eV.^[27] Finally, the F 1s spectra indicate slight dehydrofluorination of the PVDF binder during the slurry preparation process, where the released HF can further react with surface Li from the samples to form LiF (684.5 eV). [28] However, there is no significant difference between the surfaces of LNMO-P, Mg0.05-P, and Fe0.05-P before electrolyte exposure.

Following electrolyte exposure, LNMO-OCV, Fe0.05-OCV, and Mg0.05-OCV show additional surface species indicating electrolyte decomposition (Figure 3). Increases in sp³ carbon (285 eV), C-O (286 eV), O-C-O/C=O (287.8 eV), O-C=O (288.5 eV), and CO₃²⁻ (290.2 eV) are observed in the C 1s spectra, where such organic surface species originate from the decomposition of the electrolyte solvent. [27,29,30] Electrolyte salt decomposition is also observed: LiPF₆ hydrolyzes in the presence of trace water, resulting in the formation of Li/TM fluorides (LiF/TMF, 684.5 eV), Li_xPO_yF_x (534.5 eV and 686.5 eV), and Li_xPF_y species (688.5 eV), as well as an unidentified F 1s peak above 688 eV (Note S2, Supporting Information). [27,29,30] Such organic and inorganic species can also be found on the CB/PVDF-OCV electrode (Figure 3d), indicating that chemical degradation of the electrolyte occurs at the surface of CB and/or PVDF in the absence of active material or an applied current.

Carbon additives are often found to be unstable in the presence of organic electrolytes.[31-33] In this work, the CB/PVDF-OCV electrode shows a higher intensity of the LiF peak relative to the CF₂ peak when compared to LNMO-OCV, Mg0.05-OCV, and Fe0.05-OCV, which have significantly lower CB content. Since the PVDF content is the same across all electrodes, this implies that CB in the electrode promotes LiF formation/deposition. In contrast, electrodes with active material have a higher concentration of organic species, relative to the $C-C(sp^2)$ and TM-O peaks. This suggests that the presence of active material can facilitate the degradation of the electrolyte solvent, where H₂O formed as a by-product can facilitate further hydrolysis of LiPF₆.^[7] This may explain the higher concentration of Li_xPO_vF_z on the LNMO-OCV, Fe0.05-OCV, and Mg0.05-OCV surfaces when compared to CB/PVDF-OCV, since Li, PO, F, is formed through more extensive hydrolysis of the electrolyte salt than LiF. These results show that both the CB additive and the active material contribute to electrolyte degradation. The influence of CB, however, is expected to be similar for LNMO, Fe0.05, and Mg0.05.

Although salt hydrolysis occurs at each of the cathode surfaces, the $\text{Li}_x \text{PO}_y \text{F}_z$ content differs among LNMO, Fe0.05, and Mg0.05: the $\text{Li}_x \text{PO}_y \text{F}_z$ peak area (F 1s spectra) increases from LNMO-OCV < Fe0.05-OCV < Mg0.05-OCV, relative to CF₂. $\text{Li}_x \text{PO}_y \text{F}_z$ species

may improve cycling stability by scavenging dissolved TM ions and thus suppressing electrode cross-talk. [34] Such benefits to cycling performance have been demonstrated in several studies that use $\rm LiPO_2F_2$ -forming additives. [12,34] However, Li-containing additives are typically prohibitively expensive, so the ability to form $\rm Li_xPO_yF_z$ preferentially in the Mg0.05 sample would be beneficial for reducing cell costs. Nevertheless, cross-talk effects are not always obvious in LNMO|Li half-cells that have a large Li inventory, masking capacity loss caused by dissolution of active material. The direct impact of $\rm Li_xPO_yF_z$ concentrations on the cycling stability shown in Figure 1 is, therefore, unclear. However, monitoring their relative peak intensity during cycling may shed light on the degradation differences observed at each surface of the different samples.

Differences in $\text{Li}_x \text{PO}_y \text{F}_z$ relative peak intensity, as well as other inorganic species, are observed not only at OCV but also after the first cycle. For example, from Mg0.05-OCV to Mg0.05-1, the $\text{Li}_x \text{PO}_y \text{F}_z$ peak area relative to CF_2 decreases by $\approx 40\%$. This decrease, however, is more significant for LNMO ($\approx 70\%$) and Fe0.05 ($\approx 80\%$). LNMO and Fe0.05 also show a notable decrease in peak intensity for LiF and $\text{Li}_x \text{PF}_y$ species when compared to the CF_2 peak. Such dissolution of inorganic species can result from HF attack, where an increase in HF concentration is anticipated during the high-voltage operation, as demonstrated by Hestenes et al. [4,35] Greater retention of inorganic $\text{Li}_x \text{PO}_y \text{F}_z$ on the Mg0.05-1 surface, therefore, suggests that HF attack may be partially suppressed, which, in turn, could be linked to less electrolyte degradation at high voltage.

Suppression of electrolyte degradation during the first cycle in the Mg0.05 sample is corroborated by comparing the C 1s and O 1s spectra of Mg0.05-OCV and Mg0.05-1. After the first cycle, very minor differences in the organic surface layer are observed, indicating that i) the surface layer formed at OCV is stable under high-voltage operation and ii) no further degradation at the electrode surface occurs. For Fe0.05 and LNMO, on the other hand, the concentration of organic surface species decreases relative to CB (C—C, sp^2) and TM—O from OCV to the first cycle. LNMO and Fe0.05, therefore, appear to form an unstable surface layer at OCV that is partially stripped after the first cycle.

Differences in surface layer stability may be linked to differences in the composition of the surface layer itself, as LNMO-OCV and Fe0.05-OCV have a surface layer rich in carbonates and sp³ C—C functionality, whereas Mg0.05-OCV has an organic surface layer rich in C-O. This suggests that the electrolyte decomposition pathway on the Mg0.05 surface differs from that of the LNMO and Fe0.05 samples. The benefit of a C-O-rich surface has been demonstrated in other high-voltage systems. For example, Markevich et al. investigated the use of an EC-based electrolyte with and without an FEC additive in combination with a high-voltage LiCoPO₄ cathode (C/5, 3.5-5.2 V, 30 °C).^[29] They showed that without FEC, the cathode surface was rich in carbonates, while the incorporation of FEC resulted in better capacity retention, attributed to a surface layer rich in C—O functionality. While consistent with our findings, the improved oxidative stability observed in the Mg0.05 sample is somewhat surprising, given that ethers have lower oxidative stability than carbonates.^[36] The C-O-rich surface, may instead highlight the absence of reactive carbonate species such as Li₂CO₃ (section 3.2), which can promote further electrolyte degradation

16163028, 0, Downloaded from https://advanced.onlinelibrary.wiley.com/doi/10.1002/adfm.202501660 by NICE, National

Institute for Health and Care Excellence, Wiley Online Library on [10/11/2025]. See the Terms

on Wiley Online Library for rules of use; OA articles are governed by the applicable Creative Commons

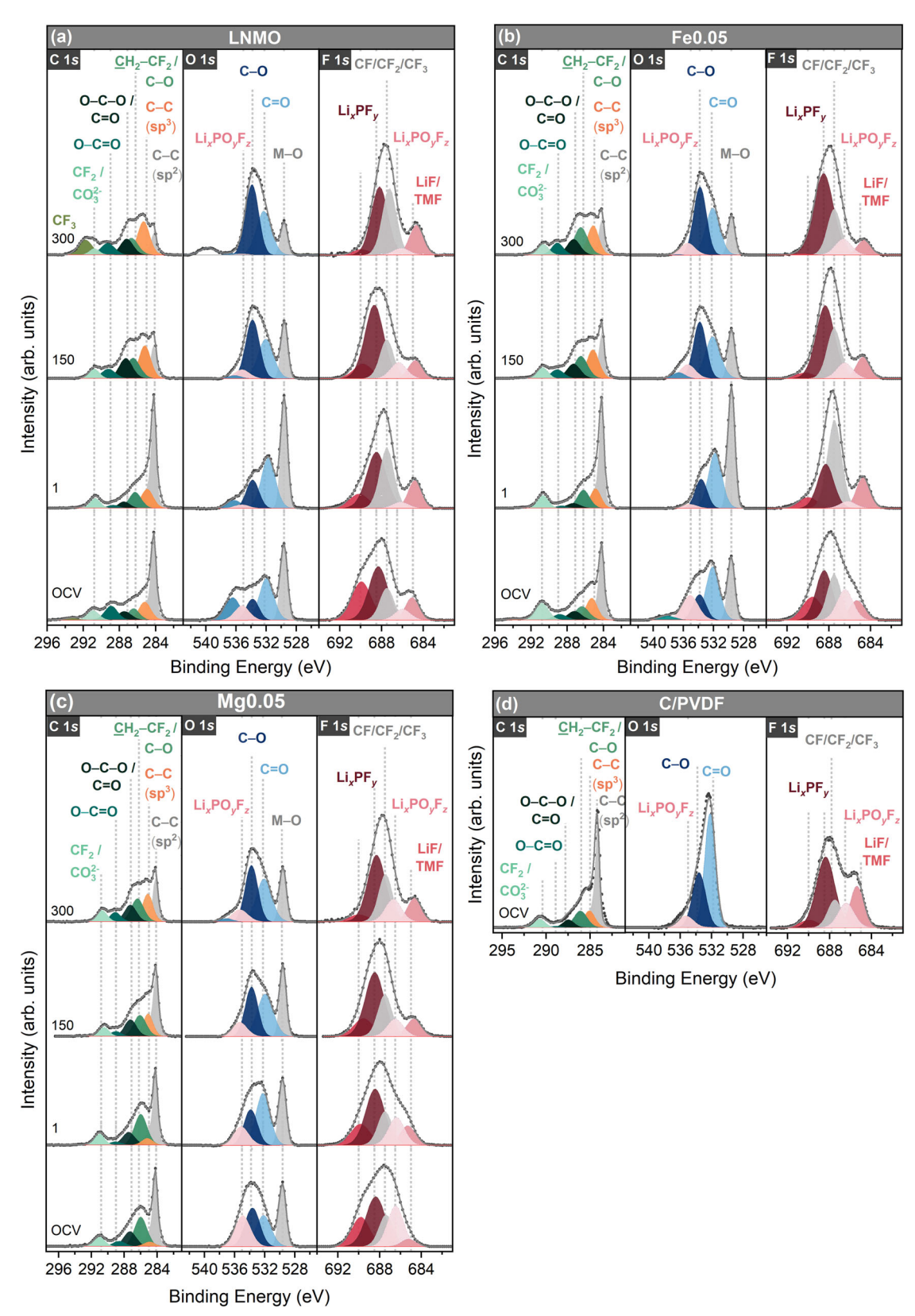


Figure 3. C 1s, O 1s, and F 1s HAXPES spectra, collected using an incident X-ray energy of 2.2 keV, for a) LNMO, b) Fe0.05, and c) Mg0.05 at various points of cycling as well as d) CB/PVDF at OCV (50 °C, 1C, 3.5–4.9 V). Electrodes for ex situ characterization were extracted before cycling (OCV) and at the end of cycles 1, 150, and 300. Spectra are area-normalized to help visualize changes in relative intensity.



www.afm-journal.de

The instability of the CEI layer is problematic for cycling stability because it exposes the electrode surface, allowing for continuous degradation and increase of degradation products. This is evident when tracking the surface layer evolution of LNMO and Fe0.05, which show a significant decrease in C-C (sp², C 1s) and TM-O (O 1s) peak intensities in comparison to the observed surface species. With prolonged cycling, there is a significant build-up of degradation products on the surface of LNMO and Fe0.05. In contrast, the relative intensity of the C-C (sp², C 1s) and TM-O (O 1s) peaks remains constant from Mg0.05-OCV to Mg0.05-150, with a slight decrease from Mg0.05-150 to Mg0.05-300. This suggests that more electrolyte degradation and CEI formation occurs at the surface of LNMO and Fe0.05 after 300 cycles at elevated temperatures, owing to the formation of an unstable surface layer that allows for continuous degradation. After prolonged cycling, the CEI layer composition is comparable across all three samples. This suggests that while the composition of the Mg0.05 surface varies during initial cycling, the processes that contribute to CEI layer thickening after long cycling are similar. This is consistent with the electrochemical analysis presented previously (Figure 1), in which the rate of capacity degradation was improved for Mg0.05 during the initial cycling but was comparable to LNMO and Fe0.05 after long cycling.

In summary, based on the HAXPES data presented, LNMO and Fe0.05 form an unstable, carbonate-rich surface layer at OCV that is partially stripped after the first cycle, most likely due to the formation of acidic species during the initial charging process. This exposes the electrode surface, allowing the CEI to continuously build up over time, consuming active material and potentially impeding Li⁺ diffusion to the electrode. CEI build-up at the Fe0.05 surface is less severe, which could explain the slight improvement in capacity retention. In contrast, the formation of a stable surface layer on Mg0.05-OCV protects the surface during initial cycling, resulting in a thinner surface layer after long-term cycling. The degradation that occurs in the later cycles, however, is expected to be similar for all samples. Mg0.05 may therefore delay degradation rather than completely prevent it. This could help to explain the improved cycling stability of Mg0.05 under accelerated aging conditions, which is most notable during initial cycling. The reason for differences in surface layer composition and formation mechanisms, however, remains unclear.

Despite literature reports demonstrating improved cycling stability with Fe-substitution in LNMO, our results show only minor improvements in capacity retention and surface stability, even at elevated temperatures. These limited improvements could be attributed to differences in synthetic methods and the resulting particle morphology. Fe-substituted materials reported in the literature typically show polycrystalline morphology (PC).[37,38] In contrast, the method adopted herein produces materials that resemble a single crystal (SC) morphology. [16] The stability of PC LNMO particles is significantly influenced by the anisotropic phase transitions that occur during cycling, which can cause particle cracking at the grain boundaries, revealing fresh surfaces and contributing to surface-related degradation mechanisms.[39] Fe substitution in PC LNMO may, therefore, alleviate particle fracture rather than electrolyte degradation, thereby indirectly limiting the extent of degradation observed. SC particles, on the other hand, are more fracture-resistant, which may limit the improvement provided by Fe in this work. Understanding how substitution influences particle fracture is an interesting direction for future investigations to understand the synthesis dependence of the enabled improvements.

3.2. Soft X-Ray Photoelectron Spectroscopy

Surface-sensitive total-electron-yield mode (TEY) with a detection depth of < 10 nm was used to investigate the evolution of the transition metal oxidation state at the surface. Throughout all stages of cycling investigated, LNMO, Fe0.05, and Mg0.05 exhibit Ni *L*-edge spectra that are consistent with that of Ni²⁺ (Figure S4, Supporting Information). The Mn *L*-edge spectra, on the other hand, have complex peak shapes that indicate the presence of Mn²⁺, Mn³⁺, and Mn⁴⁺ species (**Figure 4b–d**). The relative intensities of the Mn²⁺⁻, Mn³⁺-, and Mn⁴⁺- related peaks are identical for all three samples at OCV, with a dominant $2^+/3^+$ redox character. This suggests that, before electrochemical cycling, transition metal oxidation states at the surface are similar, despite the known differences in bulk Mn³⁺ ion content. [16]

Transition metal oxidation states are often correlated with the O *K*-edge spectra, which consist of two key features: the pre-edge (< 535 eV, peaks A and B in Figure 4a) and a broad feature above 535 eV, arising from the hybridized O *2p*-TM 4sp orbitals. [40] Figure 4a shows an additional feature at 534 eV (peak C) for LNMO and Fe0.05, which is attributed to surface Li₂CO₃. [41] Its absence in Mg0.05 may be attributed to the presence of Li-site defects, which limit the concentration of Li on the surface to subsequently form Li₂CO₃. [16] The absence of Li₂CO₃ is likely to contribute to the improved capacity retention of Mg0.05, as Li₂CO₃ on the cathode surface has been shown to enhance electrolyte degradation. [42]

The pre-edge is caused by electrons that are excited from the O 1s orbital to the unoccupied O 2p-TM 3d hybridized orbitals. [40] In LNMO spinel materials, the pre-edge represents a convolution of peaks associated with Mn—O and Ni—O bonding. As a result, the intensity of the pre-edge peaks can be affected by TM oxidation states and TM—O covalency/O 2p-TM 3d hybridization. Greater O 2p-TM 3d hybridization and orbital overlap indicate that more transitions from the O 1s to unoccupied O 2p-TM 3d hybridized orbitals are possible, resulting in a higher pre-edge peak intensity. [40] Higher TM oxidation states lead to more unoccupied O 2p-TM 3d hybridized orbitals, resulting in increased pre-edge peak intensity. [40]

The pre-edge of Mg0.05-OCV resembles that of an Mn₃O₄-like surface, which correlates well with the dominant Mn^{2+/3+} peaks observed in the corresponding Mn *L*-edge spectrum.^[4] Mn₃O₄-like surfaces are often reported to appear during the delithiation process in LNMO materials as TMs migrate into the empty tetrahedral sites.^[4,5] Recent works, however, demonstrate the presence of a Mn₃O₄-like surface in pristine LNMO samples, which can result from lithium/oxygen deficiencies that occur during synthesis.^[43] Previous structural characterization of our spinel samples revealed the presence of Li deficiencies.^[16] These Li deficiencies were most prominent in Mg-substituted samples due to the formation of Li-site defects (e.g., Mg on the Li site, Mg_{Li}). The presence of a Mn₃O₄-like surface at OCV is, therefore, most likely caused by lithium deficiencies in the Mg0.05 sample. Although all three samples have identical Mn electronic structures

16163028, 0, Downloaded from https://advanced.onlinelibrary.wiley.com/doi/10.1002/adfm.202501660 by NICE, National

Institute for Health and Care Excellence, Wiley Online Library on [10/11/2025]. See the Terms

onditions) on Wiley Online Library for rules of use; OA articles are governed by the applicable Creative Commons

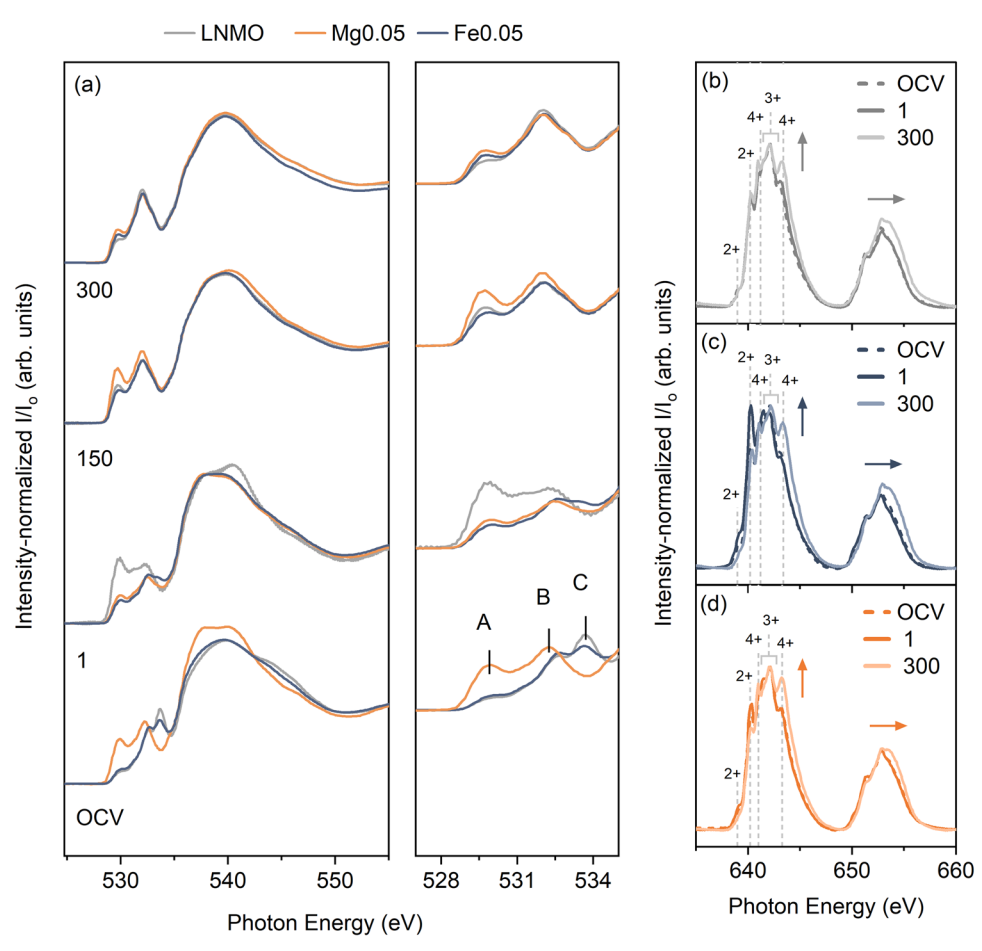


Figure 4. a) O K-edge spectra of ex situ LNMO (grev), Fe0.05 (blue), and Mg0.05 (orange) electrodes at different cycling points (50 °C, 1C, 3.5–4.9 V): before cycling (OCV) and after cycles 1, 150, and 300. Intensity-normalized Mn L-edge spectra to highlight changes in relative intensity of b) LNMO, c) Fe0.05, and d) Mg0.05.

at OCV (Figure S4b, Supporting Information), the pre-edge of LNMO-OCV and Fe0.05-OCV shows a reduced intensity for peak A (530 eV).[4] This lower intensity of peak A suggests that the overlap between the O 2p and TM 3d orbitals may be limited by factors such as local structure environment, bond strength, and covalency.

Improved O 2p-TM 3d orbital overlap in Mg0.05 may be related to the presence of Li-site defects, which are thought to prevent Mn migration into the tetrahedral sites.^[16] The orbital overlap in MnO₆ octahedra is generally stronger than in MnO₄ tetrahedra since the octahedral geometry allows the e_{σ} orbitals of Mn to point directly at the oxygen atoms, allowing for strong σ -bonding with the oxygen p orbitals. In contrast, the e_g and t_{2g} orbitals of Mn in the tetrahedral environment do not overlap as effectively, resulting in weaker bonding interactions. As a result, we expect lower pre-edge intensity. The lower pre-edge intensity of LNMO-OCV and Fe0.05-OCV may thus indicate some migration of Mn from octahedral to tetrahedral sites, reducing the overall O 2p-TM 3d hybridization. Furthermore, previous computational work on isostructural LiMn₂O₄ has shown that the presence of bulk Mn₁; defects (i.e., Mn on the tetrahedral site) does not impact the oxidation state of Mn but decreases the charge localized on oxygen.[44] This supports our observation that changes in the oxygen electronic structure and TMO, geometry can occur without changing the TM oxidation state.

Insufficient overlap of the O 2p and TM 3d orbitals is thought to limit the stability of the TM-O bonding in LNMO, allowing TM migration and dissolution. [45,46] To mitigate these processes, previous studies have successfully adopted doping strategies that aim to promote TM-O orbital hybridization in LNMO.[45,46] Liang et al. observed minimal changes in the pre-edge features (O K-edge) with cycling after Ge doping, whereas the pre-edge of LNMO changed in intensity.^[46] A similar scenario is observed for Mg0.05, which shows consistent pre-edge features throughout cycling, with slight variations in relative intensity reflecting subtle changes in the Mn oxidation state (Figure 4). Compared to Mg0.05, LNMO and Fe0.05 show significant differences in preedge features from OCV to cycle 1. This indicates that changes in the oxygen environment at the surface of LNMO and Fe0.05 are induced during the first cycle.

While enhanced O 2p-TM 3d hybridization is expected to improve the stability of the LNMO surface structure, it may also increase the nucleophilicity and thus reactivity of the surface oxygen.[47] This is evidenced by the known ability of Mg to promote oxygen redox reactions in other reported cathode materials.[48] In this work, the increased reactivity of the surface



www.afm-journal.de

oxygen in the Mg-substituted samples may explain the ability of the Mg0.05 sample to form a stable surface layer at OCV, where oxygen at the electrode surface may interact more readily with the electrolyte in the absence of an applied current. In the literature, electrolyte additives that provide nucleophilic oxygen centers are shown to promote the ring-opening polymerization of EC, forming a stable surface layer in situ.^[49,50] It is therefore possible that the increased nucleophilicity of the surface oxygen in Mg0.05 facilitates the polymerization of EC to produce a PEO-like surface layer at OCV. In this scenario, the PEO-like surface species would be covalently bonded to surface oxygen (TM—O—C), resulting in increased stability.

In addition to a stable oxygen environment, we observe that the Mn oxidation state in Mg0.05 remains stable from Mg0.05-OCV to Mg0.05-1, with negligible variation in relative peak intensity (Figure 4d). LNMO exhibits similar stability, whereas Fe0.05 shows an increase in Mn²⁺ ions during cycling (Figure 4b,c). The higher concentration of Mn²⁺ ions correlates with the increased concentration of Mn3+ ions in the Fe0.05 structure, as reported in our previous work and observed in the voltage profiles (Figure 2).[16] As a result, higher Mn3+ ion concentration contributes to greater Mn3+ ion disproportionation and Mn2+ ion deposition on the surface. [4] After 300 cycles, all samples have a similar distribution of Mn oxidation state with a relative increase in Mn⁴⁺ ion contribution (Figure 4b–d). Mn⁴⁺ ions could be formed i) to charge balance loss of active material or ii) as a product of Mn³⁺ disproportionation, forming soluble Mn²⁺ species alongside MnO₂ at the surface.^[4] The similarity in the distribution of Mn²⁺, Mn³⁺, and Mn⁴⁺ ions after 300 cycles indicates that the Mn species in all three samples experience similar degradation.

The intensity of the Mn L-edge spectral peaks (I/I_0) , without intensity normalization) for Mg0.05 is almost constant after 300 cycles (Figure S4f, Supporting Information). LNMO and Fe0.05, on the other hand, show an increase in I/Io after the first cycle, followed by a significant decrease after 300 cycles (Figure S4d,e, Supporting Information). This is consistent with the HAXPES results (Figure 3), which show an increase in peak intensity after the first cycle due to the partial stripping of the surface layer, allowing Mn within the electrode to contribute more to the observed spectra. The thick CEI layer formed after extended cycling reduces the intensity of the Mn L-edge spectra. In contrast, the stable surface layer on Mg0.05 is reflected by the stable Mn L-edge intensity. Similar changes in I/I₀ are observed in the respective Ni L-edge spectra (Figure S4g-i, Supporting Information), indicating that both Ni and Mn at the surfaces of LNMO and Fe0.05 become buried.

4. Contribution of Cell Resistance to Voltage Polarization

Due to their notable differences in electrochemical performance and surface stability, LNMO and Mg0.05 were selected for further impedance measurements to better understand the influence of surface reconstruction and CEI formation on voltage polarization and cell impedance. EIS was performed at several points during long cycling of LNMO and Mg0.05.

The typical Nyquist plot of LNMO under non-blocking conditions shows a high-frequency intercept, two semicircles in the

high- to mid-frequency region, and a tail associated with solidstate diffusion in the bulk of the electrode (Figure S5a, Supporting Information). Several studies of the impedance response in LNMO have shown that the first high-frequency semicircle, which is visible at all states of charge, is related to contact resistance. Corrosion of the current collector by HF causes the formation of insulating AlF3-like species and an increase in contact resistance during cycling.[10,23,51] Such conclusions have been reached using two-electrode half-cell and three-electrode full-cell setups in LiPF₆-based electrolytes (LP57 and LP30, respectively).[10,23,51] The high-frequency intercept of this semicircle represents solution resistance (R_{sol}), which accounts for the impedance of the electrolyte. The second semicircle, which is only evident under non-blocking conditions where charge transfer is possible (Figure S5a, Supporting Information), is a convolution of electrode pore resistance (R_{pore}) and charge-transfer resistance (R_{CT}), and is referred to as R_{cathode}.^[23]

A procedure for the deconvolution of $R_{\rm pore}$ from $R_{\rm CT}$ has been outlined in detail by Pritzl et al. $^{[23]}$ For such deconvolution, EIS data must be collected at two different points during a given cycle. The first EIS data point is collected under blocking conditions, i.e., where no charge-transfer reactions can occur. LNMO blocking conditions can be achieved by measuring EIS in the fully delithiated state (e.g., 4.9 V, Figure S5a, Supporting Information). The second EIS data point is collected under non-blocking conditions, i.e., where charge-transfer reactions can occur (e.g., 4.4 V, $\approx 10\%$ SOC, with low charge-transfer resistance). $^{[23]}$ To allow the system to reach a steady state, the aforementioned potentials were held for 1 h before the EIS measurement.

In this study, a simplified program was used in which EIS for selected cycles was only measured under non-blocking conditions (4.4 V), reducing the impact of potential hold at high voltage and ensuring reasonable correlation with surface characterization. As such, an equivalent circuit model (ECM) fitting was performed with a simple $R_{\rm sol}(R_{\rm contact}/Q_{\rm contact})(R_{\rm pore}+CT_{\rm non-blocking}/Q_{\rm pore+CT-non-blocking})Q$ circuit (Figure 5d), where the first semicircle represents $R_{\rm contact}$ and the second semicircle represents a convolution of $R_{\rm pore}$ and $R_{\rm CT}$, referred to as $R_{\rm cathode}$.

Although the model has been simplified, electrolyte degradation is expected to contribute to both $R_{\rm pore}$ and $R_{\rm CT}$; fragments from electrolyte degradation will partially block the electrode pores, reducing the effective electrolyte conductivity (increased $R_{\rm pore}$), and species deposited at the surface will impede charge transfer (increased $R_{\rm CT}$). Increases in $R_{\rm cathode}$ can, therefore, still provide information about the effects of electrolyte degradation and CEI build-up on cell impedance and voltage polarization. Finally, the tail is modeled with a constant phase element (Q) rather than a Warburg element (W), where W represents semi-infinite diffusion. $^{[52]}$ This is because the angle of the tail deviates from the idealized 45° angle. Such deviation in the tail angle indicates restricted (finite), non-ideal diffusion into the electrode. $^{[52]}$

To first demonstrate the influence of the impedance program on the recorded resistances, the simplified program (EIS@4.4 V for selected cycles) is compared to the detailed program (EIS@4.4 V+4.9 V, every cycle), with LNMO as a case study (see Experimental Methods in the Supporting Information for full details). Note that the same ECM is applied to both datasets to compare $R_{\rm sol}$, $R_{\rm contact}$, and $R_{\rm cathode}$.

of or Health and Care Excellence, Wiley Online Library on [10/11/2025]. See the Terms

nditions) on Wiley Online Library for rules of use; OA articles are governed by the applicable Creative Commons License

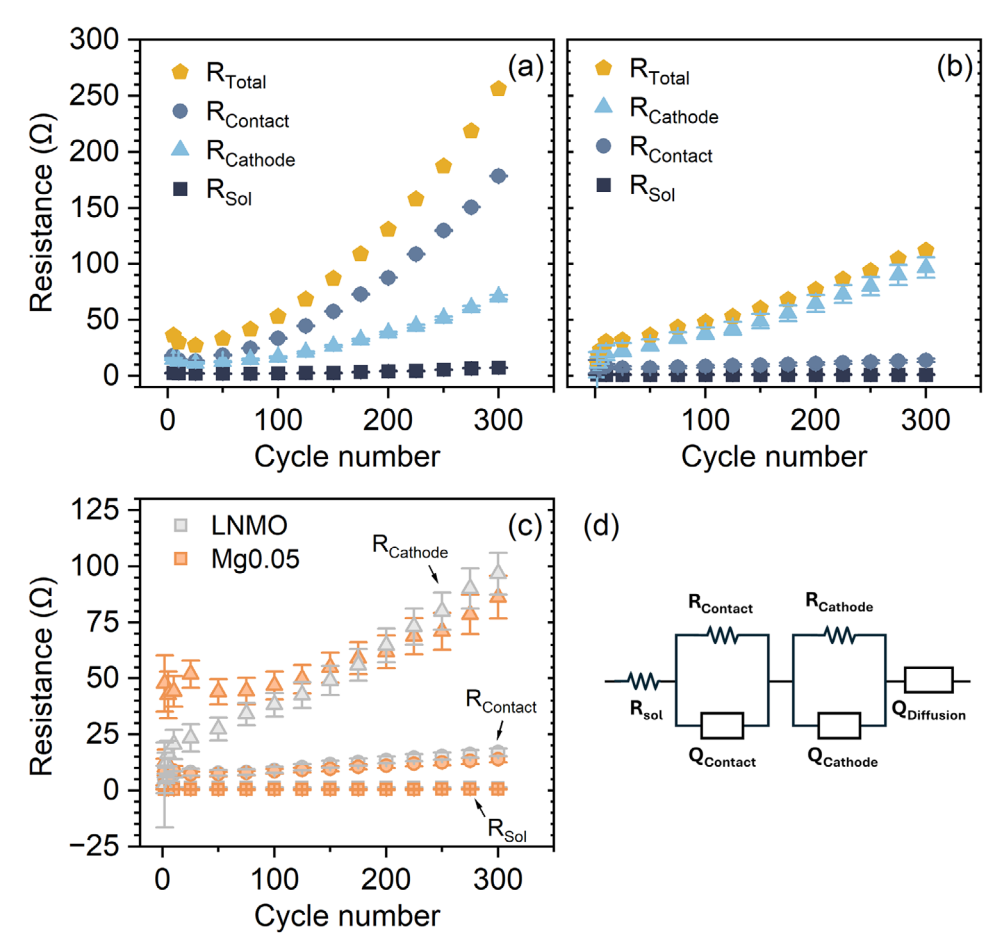


Figure 5. Resistance evolution in spinel/Li/Li three-electrode half-cells (50 °C, 1C, 3.5–4.9 V) from EIS collected at 4.4 V (discharge) for a) LNMO using the detailed program, b) LNMO using the simplified program, and c) a comparison of LNMO and Mg0.05 using the simplified program. The detailed program measures EIS at 4.9 V and 4.4 V (discharge) for each cycle, whereas the simplified program measures EIS at 4.4 V for selected cycles. Although the detailed program collects multiple datasets per cycle, only data that correspond to those collected by the simplified program are presented in (b). EIS fitting performed using the equivalent circuit model (d).

Comparing the resistance evolution when using the detailed vs. simplified program reveals two important findings: the first observation is the impact of program choice on the dominant source of resistance. When using the detailed program, the evolution of resistances correlates well with that previously reported by Pritzl et al.^[23] In this case, R_{contact} is the dominant source of resistance, R_{cathode} increased much less, and R_{sol} remained constant (Figure 5a). When the program is simplified to limit time at high voltage, R_{cathode} dominates the increases in resistance, while R_{contact} increases less and R_{sol} remains relatively constant (Figure 5b). This can be explained by the continuous formation of HF in the high-voltage region, which is known to corrode the current collector.^[10] This will be more problematic when using the detailed program, i.e., the longer time spent at high voltage, the greater R_{contact} will be compared to the simplified program. Furthermore, the CEI layer is prone to degradation and is known to be unstable in the high-voltage region.^[35] The longer time spent at high voltage is therefore expected to result in a lower R_{cathode} when using the detailed program, as the CEI degrades. When using the simplified program, protecting both the current collector and the CEI from corrosion at high voltage results in inverse contributions to resistance, lowering R_{contact} while allowing R_{cathode} to make a larger contribution.

The second observation is that the magnitude of total resistance at selected cycles is greater when using the detailed program. In this regard, we acknowledge the limitations of using a simplified program and how protecting the system from the effects of high-voltage operation will ultimately result in lower reported resistances. However, we also demonstrate the importance of matching the time scale of the impedance program to the time scale used for ex situ characterization.

The simplified program was used to monitor and compare the evolution of $R_{\rm sol},\,R_{\rm contact},\,$ and $R_{\rm cathode}$ for LNMO and Mg0.05 (Figure 5c). Both samples had relatively low and comparable $R_{\rm sol}$ and $R_{\rm contact}.$ However, notable differences in $R_{\rm cathode}$ are observed over 300 cycles. During the first 100 cycles, Mg0.05 has a higher $R_{\rm cathode}$ than LNMO, yet the magnitude of the $R_{\rm cathode}$ for Mg0.05 remains relatively constant. However, with continued cycling, Mg0.05 experiences a steady increase in $R_{\rm cathode}$ LNMO, on the other hand, shows a significantly lower $R_{\rm cathode}$ during the initial 100 cycles. However, unlike Mg0.05, LNMO experiences an increase in $R_{\rm cathode}$ that lasts throughout cycling. The rate at which

16163028, 0, Downloaded from https://advanced.onlinelibrary.wiley.com/doi/10.1002/adfm.202501660 by NICE, National Institute for Health and Care Excellence, Wiley Online Library on [101/12025]. See the Terms and Conditions (https://onlinelibrary.wiley

and-conditions) on Wiley Online Library for rules of use; OA articles are governed by the applicable Creative Commons License

R_{cathode} increases is greater for LNMO. EIS measurements correlate well with ex situ HAXPES characterization, with Mg0.05 showing a stable surface layer during the initial cycles, followed by a marginal increase in surface layer thickness after 300 cycles. The higher initial R_{cathode} for Mg0.05 is most likely due to the denser CEI that forms on the electrode surface before cycling. However, the stability of the R_{cathode} during the first 100 cycles demonstrates the protective nature of this surface, and the increase in cell impedance correlates well with the slight thickening of the CEI observed for Mg0.05-300. In contrast, the unstable surface layer observed on LNMO during initial cycling leaves the surface subject to continuous degradation, increasing R_{cathode}.

5. Conclusion

This work aims to reveal the improved stability of the cathode electrolyte interphases that form on cation-substituted LNMO cathodes, as previously hypothesized in the literature. Fe and Mg are used as Earth-abundant substituents, offering varying degrees of improvement to the capacity retention of LNMO under accelerated aging conditions, i.e., marginal improvements for Fe (88%) and more notable improvements for Mg0.05 (94%). The degradation rate for all samples was most severe during initial cycling (cycles 1-50), and while Mg and, to some extent, Fe can initially delay the degradation rate, all samples experience similar degradation in later cycles (cycles 50–300). Reduced degradation during initial cycles for Mg0.05 has many possible origins, and this work demonstrates the improved stability of the Mg0.05 surface to be one of the causes for improvement.

Changes in the oxygen electronic structure at the surface suggest that LNMO and Fe0.05 are likely to undergo some bulk/surface structural rearrangement, which is suppressed for Mg0.05. The improved surface structure for Mg0.05 could be attributed to a higher concentration of Li-site defects, which can inhibit TM migration. Longer cycling results in an increase in Mn⁴⁺ ions for all the samples (sXAS), which may be due to active material loss or Mn³⁺ ion disproportionation, leading to loss of Mn^{3+/4+}-related capacity. Ni^{2+/4+} capacity loss is also detected, along with voltage polarization, and can be attributed to changes in CEI stability and composition.

The Mg0.05 surface remains stable for the first 100 cycles, allowing for negligible changes in cell resistance and voltage polarization. The carbonate-rich CEI on LNMO and Fe0.05, on the other hand, is shown to be unstable, allowing for continued degradation, CEI build-up, and increases in cell resistance.

This work also highlights that time spent at high voltage dominates recorded contributions to cell impedance, with increased time at high voltage resulting in higher contact resistance and lower cathode resistance, most likely due to HF corrosion of both the current collector and CEI. High-voltage operation causes a significant increase in contact resistance, highlighting the need for alternative corrosion-resistant current collectors. In this work, however, where the duration at high voltage was limited, cathode resistance is dominant.

We acknowledge the limitations of the controlled nature of this study, in which half-cell testing and a limited time at high voltage mask the true effects of high-voltage degradation and TM dissolution. However, we believe that this work provides a foundation for future full-cell surface studies, allowing for the effective deconvolution of cross-talk effects as well as the surficial and cycling stability of unsubstituted, Fe-substituted, and Mgsubstituted LNMO.

Supporting Information

Supporting Information is available from the Wiley Online Library or from the author.

Acknowledgements

N.T.-R. gratefully acknowledges the Leverhulme Doctoral Scholarships Program in 'Material Social Futures' (DS-2017-036) for providing a PhD studentship to B.E.M. This work was funded by the Faraday Institution FutureCat project (FIRG065). The authors appreciate the support of Dr. Tien-Lin Lee and Dr. Pardeep Kumar Thakur at the 109 end station (Surface and Interface Structural Analysis, Diamond Light Source, UK, Proposal SI29113).

Conflict of Interest

The authors declare no conflict of interest.

Data Availability Statement

The data that support the findings of this study are available from the corresponding author upon reasonable request.

Keywords

CEI stabilization, high-voltage spinels, Li-ion battery cathodes

Received: April 11, 2025 Published online:

- [1] I. Azcarate, W. Yin, C. Méthivier, F. Ribot, C. Laberty-Robert, A. Grimaud, J. Electrochem. Soc. 2020, 167, 080530.
- [2] G. Liang, V. K. Peterson, K. W. See, Z. Guo, W. K. Pang, J. Mater. Chem. A 2020, 8, 15373.
- [3] N. P. W. Pieczonka, Z. Liu, P. Lu, K. L. Olson, J. Moote, B. R. Powell, J. H. Kim, J. Phys. Chem. C 2013, 117, 15947.
- [4] J. C. Hestenes, J. T. Sadowski, R. May, L. E. Marbella, ACS Mater. Au 2023. 3. 88.
- [5] M. Lin, L. Ben, Y. Sun, H. Wang, Z. Yang, L. Gu, X. Yu, X. Q. Yang, H. Zhao, R. Yu, M. Armand, X. Huang, Chem. Mater. 2015, 27, 292.
- [6] B. L. D. Rinkel, D. S. Hall, I. Temprano, C. P. Grey, J. Am. Chem. Soc. **2020**, 142, 15058.
- [7] Y. Liao, H. Zhang, Y. Peng, Y. Hu, J. Liang, Z. Gong, Y. Wei, Y. Yang, Adv. Energy Mater. 2024, 14, 2304295.
- [8] U. Nisar, J. Bansmann, M. Hebel, B. Reichel, M. Mancini, M. Wohlfahrt-Mehrens, M. Hölzle, P. Axmann, Chem. Eng. J. 2024, 493, 152416.
- [9] H. Wang, X. Li, F. Li, X. Liu, S. Yang, J. Ma, Electrochem. Commun. 2021, 122, 106870.
- [10] D. Pritzl, A. E. Bumberger, M. Wetjen, J. Landesfeind, S. Solchenbach, H. A. Gasteiger, J. Electrochem. Soc. 2019, 166, A582.
- [11] N. N. Intan, K. Klyukin, V. Alexandrov, J. Electrochem. Soc. 2018, 165, A1099.





www.afm-journal.de

- [12] D. Zhao, S. Song, X. Ye, P. Wang, J. Wang, Y. Wei, C. Li, L. Mao, H. Zhang, S. Li, Appl. Surf. Sci. 2019, 491, 595.
- [13] G. Liang, Z. Wu, C. Didier, W. Zhang, J. Cuan, B. Li, K. Ko, P. Hung, C. Lu, Y. Chen, G. Leniec, S. M. Kaczmarek, B. Johannessen, L. Thomsen, V. K. Peterson, W. K. Pang, Z. Guo, Angew. Chem. 2020, 132, 10681.
- [14] J. Liu, A. Manthiram, J. Phys. Chem. C 2009, 113, 15073.
- [15] L. Balducci, H. Darjazi, E. Gonzalo, R. Cid, F. Bonilla, F. Nobili, ACS Appl. Mater. Interfaces 2023, 15, 55620.
- [16] B. E. Murdock, J. Cen, A. G. Squires, S. R. Kavanagh, D. O. Scanlon, L. Zhang, N. Tapia-Ruiz, Adv. Mater. 2024, 36, 2400343.
- [17] P. Jehnichen, K. Wedlich, C. Korte, Sci. Technol. Adv. Mater. 2019, 20,
- [18] W. Bao, W. Yao, Y. Li, B. Sayahpour, B. Han, G. Raghavendran, R. Shimizu, A. Cronk, M. Zhang, W. Li, Y. S. Meng, Energy Environ. Sci. 2024. 17, 4263.
- [19] A. Tornheim, D. C. O'Hanlon, J. Electrochem. Soc. 2020, 167, 110520.
- [20] Z. Lin, T. Liu, X. Ai, C. Liang, Nat. Commun. 2018, 9, 8.
- [21] H. Arai, K. Sato, Y. Orikasa, H. Murayama, I. Takahashi, Y. Koyama, Y. Uchimoto, Z. Ogumi, J. Mater. Chem. A 2013, 1, 10442.
- [22] J. Ma, P. Hu, G. Cui, L. Chen, Chem. Mater. 2016, 28, 3578.
- [23] J. Landesfeind, D. Pritzl, H. A. Gasteiger, J. Electrochem. Soc. 2017, 164, A1773.
- [24] X. Chen, X. Wang, D. Fang, Fullerenes Nanotub. Carbon Nanostructures 2020, 28, 1048.
- [25] S. Sarkar, S. Garain, D. Mandal, K. K. Chattopadhyay, RSC Adv. 2014, 4 48220
- [26] I. A. Shkrob, D. P. Abraham, J. Phys. Chem. C 2016, 120, 15119.
- [27] S. Dalavi, M. Xu, B. Knight, B. L. Lucht, Electrochem. Solid-State Lett. 2011, 15, A28.
- [28] S. Roberts, L. Chen, B. Kishore, C. E. J. Dancer, M. J. H. Simmons, E. Kendrick, J. Colloid Interface Sci. 2022, 627, 427.
- [29] E. Markevich, G. Salitra, K. Fridman, R. Sharabi, G. Gershinsky, A. Garsuch, G. Semrau, M. A. Schmidt, D. Aurbach, Langmuir 2014, 30, 7414
- [30] E. Björklund, C. Xu, W. M. Dose, C. G. Sole, P. K. Thakur, T.-L. Lee, M. F. L. De Volder, C. P. Grey, R. S. Weatherup, *Chem. Mater.* 2022, 34, 1987
- [31] Y. H. Liu, W. C. Chen, C. H. Hsueh, C. L. Hsu, Mater. Today Chem. 2022, 25, 100934.
- [32] J. Syzdek, M. Marcinek, R. Kostecki, J. Power Sources 2014, 245, 739.
- [33] R. Younesi, A. S. Christiansen, R. Scipioni, D.-T. Ngo, S. B. Simonsen, K. Edström, J. Hjelm, P. Norby, J. Electrochem. Soc. 2015, 162, A1289.

- [34] S. Klein, P. Harte, S. van Wickeren, K. Borzutzki, S. Röser, P. Bärmann, S. Nowak, M. Winter, T. Placke, J. Kasnatscheew, *Cell Rep. Phys. Sci.* 2021. 2, 100521.
- [35] T. Yoon, J. Soon, T. Jin, J. Heon, S. M. Oh, J. Power Sources 2021, 503, 230051.
- [36] D. Ruan, Z. Cui, J. Fan, D. Wang, Y. Wu, X. Ren, Chem. Sci. 2024, 15, 4238.
- [37] F. Zou, Z. Cui, H. C. Nallan, J. G. Ekerdt, A. Manthiram, ACS Appl. Energy Mater. 2021, 4, 13297.
- [38] D. W. Shin, C. A. Bridges, A. Huq, M. P. Paranthaman, A. Manthiram, Chem. Mater. 2012, 24, 3720.
- [39] W. N. Wang, D. Meng, G. Qian, S. Xie, Y. Shen, L. Chen, X. Li, Q. Rao, H. Che, J. Liu, Y. S. He, Z. F. Ma, L. Li, J. Phys. Chem. C 2020, 124, 27937.
- [40] F. Frati, M. O. J. Y. Hunault, F. M. F. De Groot, Chem. Rev. 2020, 120, 4056.
- [41] R. Qiao, Y. De Chuang, S. Yan, W. Yang, PLoS One 2012, 7, 3.
- [42] A. T. S. Freiberg, J. Sicklinger, S. Solchenbach, H. A. Gasteiger, Electrochim. Acta 2020, 346, 136271.
- [43] X. Liu, M. Maffre, D. Tie, N. P. Wagner, N. C. Félix, R. Azmi, K. Stokes, P. E. Vullum, J. Bailly, S. Pal, G. Evans, M. Buga, M. Hahlin, K. Edström, S. Clark, A. Vlad, J. Electrochem. Soc. 2023, 170, 100527.
- [44] X. Li, J. Wang, S. Zhang, L. Sun, W. Zhang, F. Dang, H. J. Seifert, Y. Du, ACS Omega 2021, 6, 21255.
- [45] T. Fu, Y. Li, Z. Yao, T. Guo, S. Liu, Z. Chen, C. Zheng, W. Sun, Small 2024, 20, 2402339.
- [46] G. Liang, E. Olsson, J. Zou, Z. Wu, J. Li, C.-Z. Lu, A. M. D'Angelo, B. Johannessen, L. Thomsen, B. Cowie, V. K. Peterso, Q. Cai, W. K. Pang, Z. Guo, Angew. Chem., Int. Ed. 2022, 61, 202201969.
- [47] S. Myeong, W. Cho, W. Jin, J. Hwang, M. Yoon, Y. Yoo, G. Nam, H. Jang, J. G. Han, N. S. Choi, M. G. Kim, J. Cho, *Nat. Commun.* 2018, 9, 3285.
- [48] X. M. Shi, E. Watanabe, M. Okubo, A. Yamada, Chem. Mater. 2020, 32, 7181.
- [49] W.-C. Zheng, Z. Huang, C.-G. Shi, Y. Deng, Z.-H. Wen, Z. Li, H. Chen, Z. Chen, L. Huang, S.-G. Sun, ChemSusChem 2023, 16, 202202252.
- [50] J. Yang, X. Liu, Y. Wang, X. Zhou, L. Weng, Y. Liu, Y. Ren, C. Zhao, M. Dahbi, J. Alami, D. A. Ei-Hady, G.-L. Xu, K. Amine, M. Shao, Adv. Energy Mater. 2021, 11, 2101956.
- [51] C. Bizot, M. A. Blin, P. Guichard, P. Soudan, J. Gaubicher, P. Poizot, Electrochem. Commun. 2021, 126, 107008.
- [52] P. Iurilli, C. Brivio, V. Wood, J. Power Sources 2021, 505, 229860.